On-Surface Interchain Coupling and Skeletal Rearrangement of Indenofluorene Polymers

Qiang Chen, Marco Di Giovannantonio,* Kristjan Eimre, José I. Urgel, Pascal Ruffieux, Carlo A. Pignedoli, Klaus Müllen, Roman Fasel,* and Akimitsu Narita*

On-surface synthesis serves as a powerful approach to construct π-conjugated carbon nanostructures that are not accessible by conventional wet chemistry. Nevertheless, this method has been limited by the types and numbers of available on-surface transformations. While the majority of successful cases exploit thermally triggered dehalogenative carbon–carbon coupling and cyclodehydrogenation, rearrangement of appropriate functional moieties has received limited research attention. Here, the unprecedented interchain coupling and thermally induced skeleton rearrangement are described of (dihydro)indeno[2,1-*b*]fluorene (IF) polymers on an Au(111) surface under ultrahigh vacuum conditions, leading to different ladder polymers as well as fully fused graphene nanoribbon segments containing pentagonal and heptagonal rings. Au-coordinated nanoribbons are also observed. All structures are unambiguously characterized by high-resolution scanning probe microscopy. The current results provide an avenue to fabricating a wider variety of π-conjugated polymers and carbon nanostructures comprising nonhexagonal rings as well as rarely explored organometallic nanoribbons.

1. Introduction

Controlling structures and properties of carbon-based π-conjugated nanostructures by the rational design of molecular precursors holds promise for applications in advanced electronic and optoelectronic devices.[1] In particular, quasi-one-dimensional graphene nanoribbons (GNRs), i.e., nanoscale strips of graphene, and more generally π-conjugated ladder polymers (CLPs), consisting of two or more interconnected polymer strands, have attracted increasing attention.[2] Compared to extensively investigated GNRs consisting only of benzene rings, "defective" GNRs or CLPs containing nonhexagonal rings, e.g., pentagonal and heptagonal rings,[3] offer a larger structural diversity and exhibit highly intriguing properties, such as narrower energy gaps,[3c,4] higher charge-carrier mobility,[5] intrinsic dipolar moments,[3b]

Q. Chen, K. Müllen, A. Narita
Max Planck Institute for Polymer Research Ackermannweg 10
D-55128 Mainz, Germany
E-mail: narita@mpip-mainz.mpg.de

Q. Chen
Institute of Functional Nano & Soft Materials (FUNSOM)
Joint International Research Laboratory of Carbon-Based Functional Materials and Devices
Jiangsu Key Laboratory for Carbon-Based Functional Materials & Devices
Soochow University
Suzhou, Jiangsu 215123, P. R. China

M. Di Giovannantonio, K. Eimre, J. I. Urgel, P. Ruffieux, C. A. Pignedoli, R. Fasel
Swiss Federal Laboratories for Material Science and Technology
Dübendorf 8600, Switzerland
E-mail: marco.digiovannantonio@ism.cnr.it; roman.fasel@empa.ch

M. Di Giovannantonio
Institute of Structure of Matter – CNR (ISM-CNR)
Rome 00133, Italy

J. I. Urgel
IMDEA Nanoscience
C/ Faraday 9
Campus de Cantoblanco
Madrid 28049, Spain

K. Müllen
Department of Chemistry
Johannes Gutenberg University Mainz
D-55128 Mainz, Germany

R. Fasel
Department of Chemistry
Biochemistry and Pharmaceutical Sciences
University of Bern
Bern 3012, Switzerland

A. Narita
Organic and Carbon Nanomaterials Unit
Okinawa Institute of Science and Technology Graduate University
Kunigami-gun, Okinawa 904-0495, Japan

ADVANCED
SCIENCE NEWS

www.advancedsciencenews.com

[M] acro-
molecular
Chemistry and Physics

www.mcp-journal.de
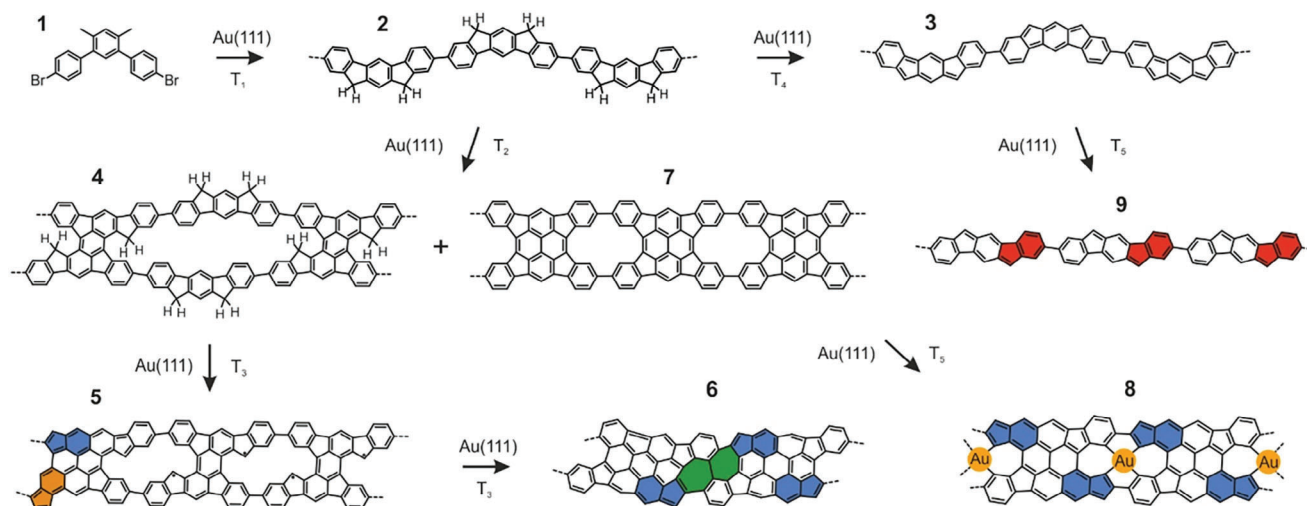
Scheme 1. Reaction scheme towards indeno[2,1-*b*]fluorene polymer **3** on Au(111) and various product structures observed at different temperatures. The on-surface reaction temperatures are $T_1 = 250\ °C$, $T_2 = 310\ °C$, $T_3 = 420\ °C$, $T_4 = 360\ °C$, and $T_5 = 480\ °C$. At T_1, **2** is the main product, while different products coexist at the other temperatures (at T_2, **2**, **4**, and **7**; at T_3, **3** and **5**–**7**; at T_4, **2**–**7**; at T_5, **3** and **5**–**9**). See Table 1 for the yields of the observed products.

and open-shell characters.[6] Such nonbenzenoid structures are, however, underexplored.

On-surface synthesis has recently emerged as an approach toward the fabrication of low dimensional π-conjugated carbon nanostructures with atomic precision.[7] This nonconventional synthetic method mainly relies on thermally induced dehalogenative coupling[8] and oxidative cyclodehydrogenation[9] on atomically flat metal surfaces, such as Au(111) and Ag(111). The distinct advantage of this protocol over the conventional solution synthesis is that even highly unstable and insoluble products become accessible under ultrahigh vacuum (UHV) conditions. Therefore, materials which would not survive in solution can thus be fabricated and characterized in situ by scanning probe microscopy (SPM) and different surface spectroscopy methods, such as X-ray photoelectron spectroscopy (XPS) and scanning tunneling spectroscopy (STS).[7c,10] In the past decade, various GNRs and other polymers were synthesized on surface based on clever designs of halogenated molecular precursors.[10g,11] While carbon–carbon coupling and cyclization reactions have been predominantly utilized, skeletal rearrangements have also been occasionally observed on surface,[12] paving the way to unprecedented nonbenzenoid structures that are otherwise unattainable. However, reported examples of on-surface rearrangement reactions are still scarce[12d,13] and rarely provided one-dimensionally extended CLPs or GNRs with regular incorporation of nonhexagonal rings.[12a]
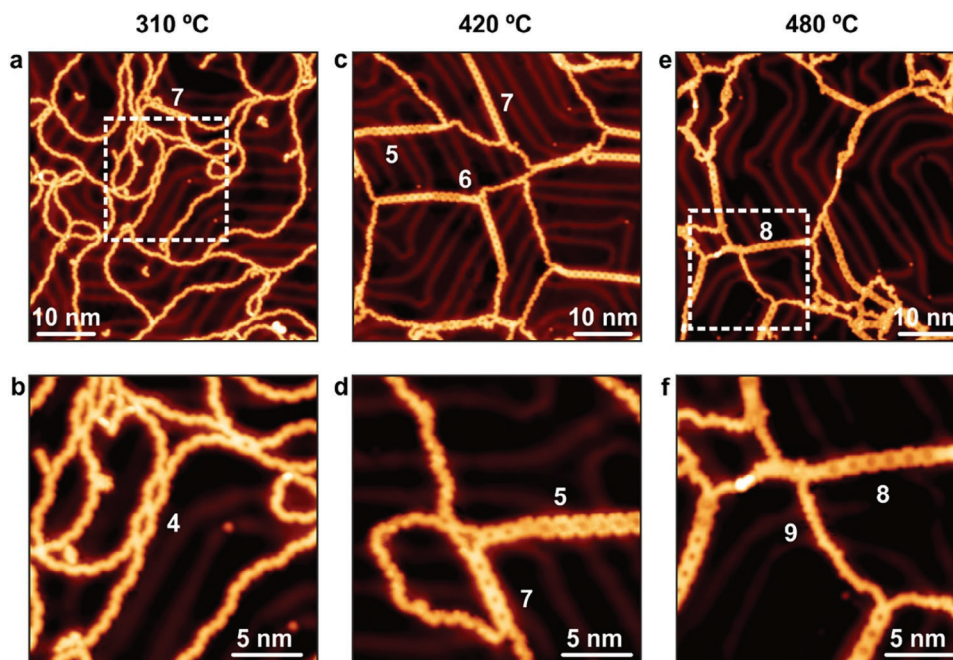
Indenofluorenes typically have linearly fused and fully conjugated 6-5-6-5-6 ring systems with antiaromaticity and diradical characters.[6a,14] Among them, indeno[2,1-*b*]fluorene (IF) shows high open-shell diradical character. We recently reported the on-surface synthesis of IF polymer **3** through the formation of pentagonal rings by the oxidative cyclization of methyl groups, using 4,4′′′-dibromo-4′,6′-dimethyl-1,1′:3′,1′′′-terpheny (**1**) as the precursor (**Scheme 1**).[6a] Moreover, we disclosed the interchain coupling of dihydroindeno[2,1-*b*]fluorene (2H-IF) polymer **2** into ladder-type porous nanoribbon **7**, consisting of tetraindenopy-

rene as the repeating unit. However, there were also some distinct porous nanoribbon structures with different pore sizes, which remained unclear. In this work, we unambiguously elucidate the precise chemical structures of such porous nanoribbons as **4** and **5** by high-resolution scanning tunneling microscopy (STM) and noncontact atomic force microscopy (nc-AFM) at low temperature under UHV, demonstrating the interchain coupling at different positions as well as occurrence of skeletal rearrangement. Moreover, we increased the annealing temperature up to 480 °C and discovered the formation of intriguing nonbenzenoid GNR segment **6** with heptagonal rings as well as unprecedented Au-coordinated GNR **8**. Based on our observations, we propose a possible reaction mechanism of the skeletal rearrangement involving thermally induced ring-opening of the IF backbone, followed by Garratt–Braverman cyclization.

2. Results and Discussion

2.1. On-Surface Synthesis and Elucidation of Product Structures

The on-surface synthesis and characterizations of IF polymer **3** and porous nanoribbon **7** from precursor **1** are described in detail in our previous report.[6a] **Figure 1** shows representative STM images of reaction products on the Au(111) surface after deposition of precursor **1** at room temperature and subsequent annealing to the indicated temperatures. After annealing at 310 °C, some parts of the polymer chains, mainly consisting of 2H-IF polymer **2**, laterally fused to form previously identified porous nanoribbon **7** and another porous nanoribbon structure **4** with larger pores (Figure 1a,b). Through the constant-height frequency shift nc-AFM analysis with a carbon monoxide (CO)-functionalized tip,[15] the chemical structure of the latter could be clearly resolved as displayed in **Figure 2**a. The nc-AFM image of the fused unit of **4** clearly revealed higher contrasts at the apexes of the pentagonal rings that were apparently not involved in the benzene ring formation, which could be assigned to out-of-plane C–

ADVANCED
SCIENCE NEWS

www.advancedsciencenews.com

Macromolecular
Chemistry and Physics

www.mcp-journal.de

310 °C   420 °C   480 °C

Figure 1. Overview STM images after annealing the sample on the Au(111) surface to different temperatures. a,b) Surface after annealing the sample to 310 °C. The white dashed line in panel a indicates the zoom-in region of panel (b). c,d) Surface after annealing the sample to 420 °C. e,f) Surface after annealing the sample to 480 °C. The white dashed line in panel e indicates the zoom-in region of panel (f). Some of the structures of interest are indicated with numbers corresponding to those displayed in Scheme 1. The images were recorded on different samples and areas with varying molecular coverages. Scanning parameters: a,b) $V_b = -0.30$ V, $I_t = 0.05$ nA; c,d) $V_b = -0.30$ V, $I_t = 0.02$ nA; e) $V_b = -0.50$ V, $I_t = 0.05$ nA; f) $V_b = -0.25$ V, $I_t = 0.05$ nA.
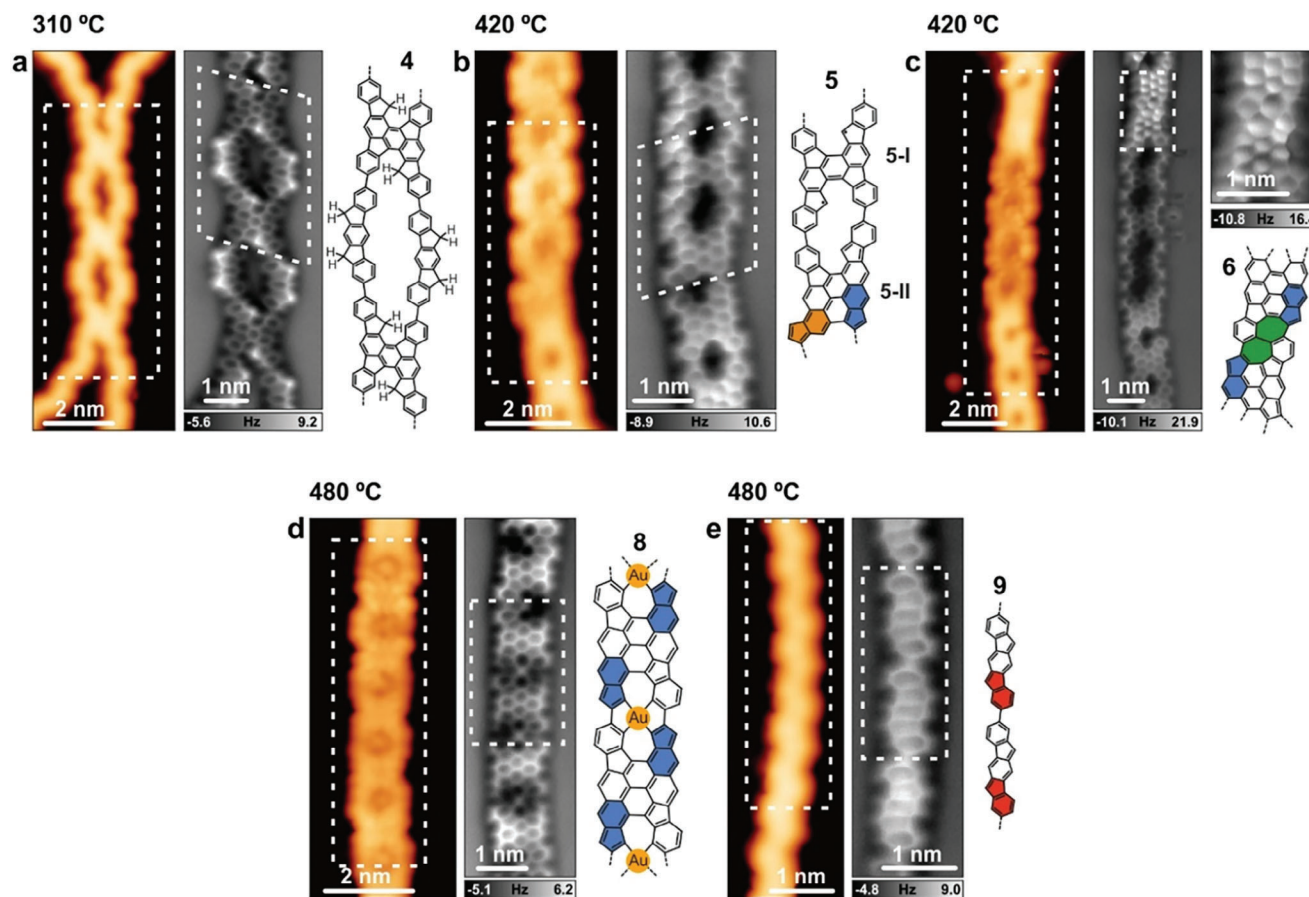
H bonds on sp^3 carbons of these cyclopentadiene rings. While porous nanoribbon **7** resulted from the symmetrical fusion of two strands of 2H-IF polymer **2**, involving all of the 2H-IF units, the observed structure of porous nanoribbon **4** indicated fusion in a staggered manner, leaving every second 2H-IF units unreacted, presumably due to an enhanced kinetic energy barrier with a larger strain. The occurrence of this asymmetrical fusion can be ascribed to limited mobility of the polymer chains, forming only one benzene ring between the two 2H-IF units due to the "mismatch", in contrast to the two rings formed in the case of symmetrical fusion to **7**.

After annealing of the sample to 420 °C, STM and nc-AFM analyses revealed the disappearance of **4** and formation of another porous nanoribbons **5** with varying pore sizes, indicating further chemical transformations of **4** (Figures 1c,d and 2b). All the unreacted 2H-IF units in **4** were fused together in **5** and the nc-AFM image of the latter displayed its highly planar structure without any out-of-plane C–H bond assignable to an sp^3 carbon. In addition to the structural unit **5-I** with two directly fused IFs (upper part of the ribbon **5** in Figure 2b), we also observed the structural unit **5-II**, where the 6-5-6-5-6 ring systems originating from indeno[2,1-*b*]fluorene were transformed to indeno[5,6-*b*]fluorene and indeno[5,4-*b*]fluorene substructures with 6-5-6-6-5 ring systems, indicating skeletal rearrangements (highlighted in blue in Scheme 1 and Figure 2b). The apices of the five-membered rings appear lower in the nc-AFM image most likely due to their strong interaction with the gold substrate, as previously observed and discussed for IF polymer **3**.[6a] Notably, we also observed fully fused segments without any pore, and

nc-AFM analysis of one of them elucidated nonbenzenoid GNR structure **6** with incorporated heptalene, namely two neighboring seven-membered rings, formed through an additional C–C bond formation between the repeating units enabled by suitable ring rearrangements (highlighted in green in Scheme 1 and Figure 2c, see Scheme S1 in the Supporting Information for proposed formation mechanism).

Further annealing of the sample to 480 °C induced significant modifications in the observed structures (Figure 1). While some porous nanoribbons **7** were still observed, the STM and nc-AFM analyses (Figure 2d) clearly revealed the presence of nanoribbons with a distinct contrast and circular features decorating the pores (**8**), which were ascribed to the coordination of gold atoms from the substrate. Interestingly, such Au-coordination was not observed for every type of pore but only in rearranged ones, where Au can be coordinated to two five- and two six-membered rings or occasionally one five- and three six-membered rings. Organometallic Au complexes have rarely been observed on surface, except for some limited cases where steric hindrance plays a role,[16] in contrast to Ag and Cu with more examples of organometallic structures coordinating surface adatoms.[17] On the other hand, some single strand polymers were also present on the same sample, probably due to their reduced mobility in light of the "pinning" of their ends through the interchain couplings. Nc-AFM analysis of some of these single-strand segments revealed the isomerization of indeno[2,1-*b*]fluorene polymer **3** to indeno[1,2-*b*]fluorene polymer **9** (highlighted by filled red rings in Scheme 1 and Figure 2e), in agreement with theoretical result indicating higher thermodynamic stability of the latter

**ADVANCED
SCIENCE NEWS**

www.advancedsciencenews.com

**[M] acro- olecular
Chemistry and Physics**

www.mcp-journal.de

Figure 2. High resolution STM images (orange color scale) of various observed products with the corresponding nc-AFM images (grey color scale) and chemical structures. a) Porous nanoribbon segment **4**. b) Porous nanoribbon **5**, consisting of different rearranged (highlighted in blue and orange) or non-rearranged structures. c) Nanoribbon with a fully fused segment **6**, where seven-membered rings are formed (highlighted in green). d) Au-incorporated nanoribbon **8**. e) Polymer **9** with indeno[1,2-*b*]fluorene units (rearranged rings highlighted in red). The annealing temperature of the Au(111) substrate are indicated for each panel. The white dashed lines in the STM images indicate the zoom-in area where the nc-AFM images were acquired. The white dashed lines in the nc-AFM images indicate the segments represented in the chemical structures. Scanning parameters: (a) $V_b = -0.30$ V, $I_t = 0.05$ nA; (b) $V_b = -0.30$ V, $I_t = 0.02$ nA; (c) $V_b = -0.20$ V, $I_t = 0.03$ nA; (d,e) $V_b = -0.02$ V, $I_t = 0.15$ nA.

(see below and Figure S1 in the Supporting Information). Additionally, some segments of the single-strand chains appeared different from the above-described structures **2**, **3**, and **9**. We employed nc-AFM imaging to resolve the chemical structure of one of them, and observed pentalene, consisting of two neighboring five-membered rings (highlighted in magenta), arising from ring rearrangement at this high temperature (**Figure 3**; see Scheme S1 in the Supporting Information for proposed formation mechanism). Moreover, we also observed a unique cyclopenta[*a*]pentalene substructure with three consecutive pentagons (highlighted in cyan) and extended ladder oligomer structure with at least 14 consecutively fused rings.

2.2. Statistical Analysis of the Products

To elucidate the temperature dependence of the interchain coupling and isomerization processes, we performed statistical analysis of the different product structures **2–9** at each temperature based on STM images, although additional single-strand poly-

mers different from **2**, **3**, and **9** could not be distinguished without nc-AFM images (**Table 1**). One of the most significant features is that while increasing the temperature from 310 up to 420 °C, the percentage of single-strand polymers drastically decreased from 76% (all of type **2**) to 40% (mainly of type **3**), giving rise to porous nanoribbons **5** (9%) and to a significant increase of **7** (43%). We also notice the presence of fully fused segments **6** (8%). At 480 °C, the isomers **5** almost disappear with the total percentage being less than 1% and the main products are single chains (37%), which are composed of indeno[2,1-*b*]fluorene (**3**) and indeno[1,2-*b*]fluorene (**9**), as well as the fully planarized tape **6** containing heptagonal and pentagonal rings (28%) and organometallic complex **8** (26%).
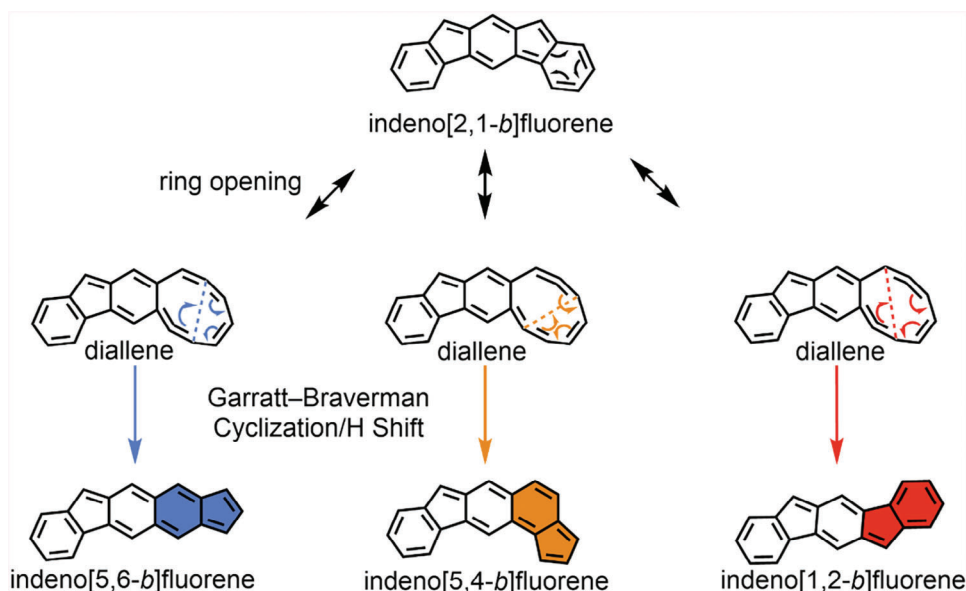
2.3. Proposed Rearrangement Mechanism

We propose an isomerization mechanism that can explain the formation of three indenofluorene regioisomers, which appear as substructures in products **5**, **6**, **8**, and **9**. At an elevated temper-
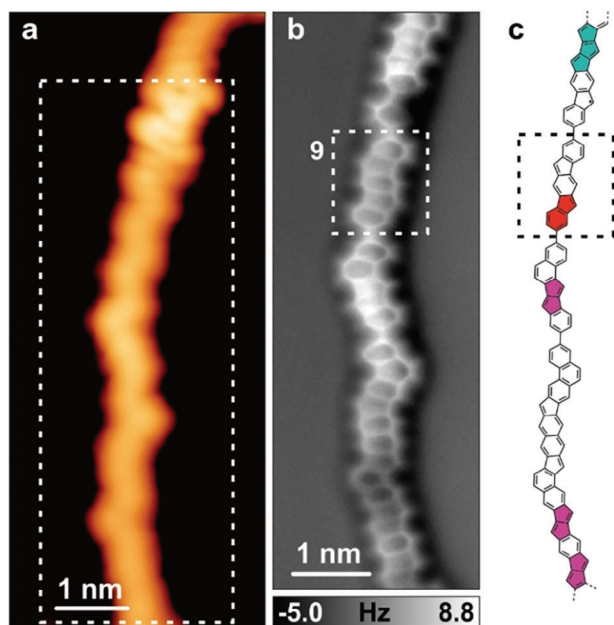
Figure 3. High resolution a) STM and b) nc-AFM images of a polymeric chain observed on Au(111) after annealing to 480 °C, with the chemical structure assigned as shown in panel (c). One unit of structure **9** is bonded to other irregularly rearranged structural units with pentalene (magenta) and cyclopenta[*a*]pentalene (cyan) substructures. Scanning parameters: (a) $V_b = -0.20$ V, $I_t = 0.15$ nA.

Table 1. Yields (in percentage) of the observed products at the investigated temperatures.

	310 °C[a]	360 °C[a]	420 °C[a]	480 °C[a]
4	3	1	0	0
5	0	14	9	1
6	0	1	8	28
7	21	35	43	9
8	0	0	0	26
Single chains	76 (all **2**)	49 (**2**: 76, **3**: 24)	40 (mainly **3**)	36 (**3** + **9** + others[b])

[a] The number of monomers in a specific configuration has been evaluated from the STM images. The percentages have been obtained after counting over more than 3000 monomers for the phases at 310, 360, and 420 °C and over more than 600 monomers for the phase at 480 °C; [b] At this temperature it is not possible to distinguish the chemical structure of the single chains from STM solely if they differ from the known appearance of **3** and **9**. Therefore, a precise estimation of the relative abundances is not possible.

ature, an IF unit presumably undergoes ring opening[13a] at the terminal six-membered ring on Au(111), affording a metastable diallene intermediate (**Scheme 2**). Such diallene can again form fused pentagonal and hexagonal ring pair via Garratt–Braverman cyclization.[18] The geometry of these two rings is determined

by the positions of the carbon atoms involved in the reaction, causing the isomerization, which can also account for the formation of the pentalene and heptalene substructures discussed above (Scheme S1, Supporting Information). We computed the total energy of the four types of molecular units present in **3**, **5**, and **9** adsorbed on Au(111) (Figure S1, Supporting Information). DFT-optimized geometries reveal that indeno[1,2-*b*]fluorene as in **9** is 0.23 eV more stable than indeno[2,1-*b*]fluorene in **3**, rationalizing the experimental observation of the former after annealing the latter at 480 °C. Namely, **9** is the thermodynamically most stable product in the case of single-strand polymers. Such skeletal rearrangement thus promoted the formation of molecular units with a decreased diradical character.[19] On the other hand, comparing the two observed 6-5-6-6-5 ring systems (e.g., in **5**), the linear indeno[5,6-*b*]fluorene is more stable than the

Scheme 2. Proposed mechanism of the ring rearrangement. The indeno[2,1-*b*]fluorene species undergo ring opening and form ene-diallene metastable intermediates. Depending on the carbon atoms involved in the closure of the 9-membered ring, three different products can be achieved via Garratt–Braverman cyclization followed by hydrogen migration.

**ADVANCED
SCIENCE NEWS**

www.advancedsciencenews.com

[M]acro-
molecular
Chemistry and Physics

www.mcp-journal.de

U-shaped indeno[5,4-*b*]fluorene, both showing higher energy as compared to the starting indeno[2,1-*b*]fluorene in **3** (0.15 and 0.20 eV for indeno[5,6-*b*]fluorene and indeno[5,4-*b*]fluorene, respectively, see Figure S1, Supporting Information). The highest energy of indeno[5,4-*b*]fluorene among the four isomers is consistent with its very rare experimental observation of this structure.

3. Conclusion

In summary, we have reported a new type of thermally induced skeleton rearrangement of IF units fixed in polymer chains on an Au(111) surface. Three types of isomers were unambiguously identified by high-resolution scanning probe microscopy. Based on these observations, the rearrangement mechanism was proposed and the entire reaction was supposed to go through routes that resemble retro-Bergman reaction involving ring opening of indene on one termini of the IF unit and subsequent closure involving three different pairs of carbon atoms, affording three final isomers. The single chains underwent lateral fusion to provide π-conjugated ladder polymers of various types, including incorporation of heptagonal and pentagonal rings. The partially fused polymers that could not undergo further ring closure due to the long distance between corresponding carbon atoms, featured an unusual Au intercalation into the ribbon backbone, and four covalent C–Au bonds were formed for each repeating unit. We envisage that the skeleton rearrangement strategy reported herein will enable the preparation of many other structural complex nonbenzenoid conjugated polymers through rational design of precursors and reaction routes. Our results provide a new strategy to synthesize CLPs and GNRs with non-benzenoid backbones and metal atom intercalation using structurally simple precursors.

4. Experimental Section

STM and nc-AFM Experiments: The on-surface synthesis experiments were performed under ultrahigh vacuum (UHV) conditions with base pressure below 2×10^{-10} mbar. Au(111) substrates (MaTeck GmbH) were cleaned by repeated cycles of Ar$^+$ sputtering (1 keV) and annealing (460 °C). The precursor molecules were thermally evaporated onto the clean Au(111) surface from a quartz crucible heated at 60 °C with a deposition rate of $\approx$0.5 Å min^{-1}. STM images were acquired with a low-temperature scanning tunneling microscope (Scienta Omicron) operated at 5 K in constant-current mode using an etched tungsten tip. Bias voltages are given with respect to the sample. nc-AFM measurements were performed at 5 K with a tungsten tip placed on a qPlus force sensor.[20] The tip was functionalized with a single CO molecule at the tip apex picked up from the previously CO-dosed surface.[15a] The sensor was driven at its resonance frequency (27 050 Hz) with a constant amplitude of 70 pm. The frequency shift from resonance of the tuning fork was recorded in constant-height mode using Omicron Matrix electronics and HF2Li PLL by Zurich Instruments.

Computational Details: Density functional theory (DFT) calculations were conducted using the AiiDAlab platform[21] and AiiDA workflows[22] based on the CP2K code.[23] To model the surface–adsorbate systems, the repeated slab scheme was employed. The simulation cell comprised four atomic layers of gold oriented along the [111] direction. To suppress the Au(111) surface state, one side of the slab was passivated with a layer of hydrogen atoms. Additionally, a 40 Å vacuum region was included in the simulation cell to isolate the system from its periodic replicas in the direction perpendicular to the surface.

For electronic state expansion, a TZV2P Gaussian basis set[24] was utilized for carbon and hydrogen species, while a DZVP basis set was employed for gold species. The plane-wave basis set had a cutoff of 600 Ry. To account for the frozen core electrons of the atoms, norm-conserving Goedecker–Teter–Hutter pseudo-potentials were used.[25] The Perdew–Burke–Ernzerhof parameterization was applied for the generalized gradient approximation of the exchange-correlation functional.[26] Van der Waals interactions were considered using the D3 scheme proposed by Grimme.[27]

The gold surface was modeled using a super-cell with dimensions of 29.5×30.6 Å^2, equivalent to 120 surface unit cells. The Au(111) slab was treated as planar, and the herringbone reconstruction associated with this surface was not considered, as it would significantly increase the supercell size without substantially altering the chemical activity of the surface.[28]

To obtain equilibrium geometries, the atomic positions of the bottom two layers were held of the slab fixed at their ideal bulk positions, while allowing all other atoms to relax until the forces on them were below 0.005 eV Å^{-1}.

Supporting Information

Supporting Information is available from the Wiley Online Library or from the author.

Conflict of Interest

The authors declare no conflict of interest.

Data Availability Statement

The data that support the findings of this study are available from the corresponding author upon reasonable request.

[1] a) Z. Chen, A. Narita, K. Müllen, *Adv. Mater.* **2020**, *32*, 2001893; b) H. Wang, H. S. Wang, C. Ma, L. Chen, C. Jiang, C. Chen, X. Xie, A.-P. Li, X. Wang, *Nat. Rev. Phys.* **2021**, *3*, 791; c) R. S. K. Houtsma, J. De La Rie, M. Stöhr, *Chem. Soc. Rev.* **2021**, *50*, 6541.

[2] a) C. Zhu, A. J. Kalin, L. Fang, *Acc. Chem. Res.* **2019**, *52*, 1089; b) J. Lee, A. J. Kalin, T. Yuan, M. Al-Hashimi, L. Fang, *Chem. Sci.* **2017**, *8*, 2503; c) J. Lee, *Asian J. Org. Chem.* **2023**, *12*, 202300104.

[3] a) J. I. Urgel, J. Bock, M. Di Giovannantonio, P. Ruffieux, C. A. Pignedoli, M. Kivala, R. Fasel, *RSC Adv.* **2021**, *11*, 23437; b) Q. Fan, D. Martin-Jimenez, D. Ebeling, C. K. Krug, L. Brechmann, C. Kohlmeyer, G. Hilt, W. Hieringer, A. Schirmeisen, J. M. Gottfried, *J. Am. Chem. Soc.* **2019**, *141*, 17713; c) B. De La Torre, A. Matej, A. Sánchez-Grande, B. Cirera, B. Mallada, E. Rodríguez-Sánchez, J. Santos, J. I. Mendieta-Moreno, S. Edalatmanesh, K. Lauwaet, M. Otyepka, M. Medved, Á. Buendía, R. Miranda, N. Martín, P. Jelínek, D. Écija, *Nat. Commun.* **2020**, *11*, 4567.

[4] A. Jiménez-Martín, F. Villalobos, B. Mallada, S. Edalatmanesh, A. Matej, J. M. Cuerva, P. Jelínek, A. G. Campaña, B. De La Torre, *Chem. Sci.* **2023**, *14*, 1403.

[5] A. Babel, S. A. Jenekhe, *J. Am. Chem. Soc.* **2003**, *125*, 13656.

[6] a) M. Di Giovannantonio, K. Eimre, A. V. Yakutovich, Q. Chen, S. Mishra, J. I. Urgel, C. A. Pignedoli, P. Ruffieux, K. Müllen, A. Narita, R. Fasel, *J. Am. Chem. Soc.* **2019**, *141*, 12346; b) P. Hu, S. Lee, T. S. Herng, N. Aratani, T. P. Gonçalves, Q. Qi, X. Shi, H. Yamada, K.-W. Huang, J. Ding, D. Kim, J. Wu, *J. Am. Chem. Soc.* **2016**, *138*, 1065.

[7] a) S. Clair, D. G. De Oteyza, *Chem. Rev.* **2019**, *119*, 4717; b) A. Narita, Z. Chen, Q. Chen, K. Müllen, *Chem. Sci.* **2019**, *10*, 964; c) L. Grill, S. Hecht, *Nat. Chem.* **2020**, *12*, 115.

[8] a) L. Grill, M. Dyer, L. Lafferentz, M. Persson, M. V. Peters, S. Hecht, *Nat. Nanotechnol.* **2007**, *2*, 687; b) M. Lackinger, *Chem. Commun.* **2017**, *53*, 7872; c) S. Stolz, M. Di Giovannantonio, J. I. Urgel, Q. Sun, A. Kinikar, G. Borin Barin, M. Bommert, R. Fasel, R. Widmer, *Angew. Chem., Int. Ed.* **2020**, *59*, 14106.

[9] M. Treier, C. A. Pignedoli, T. Laino, R. Rieger, K. Müllen, D. Passerone, R. Fasel, *Nat. Chem.* **2011**, *3*, 61.

[10] a) T. Wang, J. Zhu, *Surf. Sci. Rep.* **2019**, *74*, 97; b) Q. Shen, H.-Y. Gao, H. Fuchs, *Nano Today* **2017**, *13*, 77; c) A. Sweetman, N. R. Champness, A. Saywell, *Chem. Soc. Rev.* **2020**, *49*, 4189; d) L. Dong, P. N. Liu, N. Lin, *Acc. Chem. Res.* **2015**, *48*, 2765; e) Q. Fan, J. M. Gottfried, J. Zhu, *Acc. Chem. Res.* **2015**, *48*, 2484; f) R. Lindner, A. Kühnle, *ChemPhysChem* **2015**, *16*, 1582; g) S. Song, J. Su, M. Telychko, J. Li, G. Li, Y. Li, C. Su, J. Wu, J. Lu, *Chem. Soc. Rev.* **2021**, *50*, 3238; h) M. Lackinger, *Trends Chem.* **2022**, *4*, 471; i) S. Stolz, M. Di Giovannantonio, O. Gröning, R. Widmer, *Chimia* **2022**, *76*, 203.

[11] a) A. Kinikar, M. Di Giovannantonio, J. I. Urgel, K. Eimre, Z. Qiu, Y. Gu, E. Jin, A. Narita, X.-Y. Wang, K. Müllen, P. Ruffieux, C. A. Pignedoli, R. Fasel, *Nat. Synth.* **2022**, *1*, 289; b) X. Yu, L. Cai, M. Bao, Q. Sun, H. Ma, C. Yuan, W. Xu, *Chem. Commun.* **2020**, *56*, 1685; c) P. Ruffieux, S. Wang, B. Yang, C. Sánchez-Sánchez, J. Liu, T. Dienel, L. Talirz, P. Shinde, C. A. Pignedoli, D. Passerone, T. Dumslaff, X. Feng, K. Müllen, R. Fasel, *Nature* **2016**, *531*, 489; d) C. Moreno, M. Vilas-Varela, B. Kretz, A. Garcia-Lekue, M. V. Costache, M. Paradinas, M. Panighel, G. Ceballos, S. O. Valenzuela, D. Peña, A. Mugarza, *Science* **2018**, *360*, 199; e) X. Li, H. Zhang, L. Chi, *Adv. Mater.* **2018**, *31*, 1804087.

[12] a) I. C.-Y. Hou, Q. Sun, K. Eimre, M. Di Giovannantonio, J. I. Urgel, P. Ruffieux, A. Narita, R. Fasel, K. Müllen, *J. Am. Chem. Soc.* **2020**, *142*, 10291; b) X. Xu, M. Di Giovannantonio, J. I. Urgel, C. A. Pignedoli, P. Ruffieux, K. Müllen, R. Fasel, A. Narita, *Nano Res.* **2021**, *14*, 4754; c) O. Stetsovych, M. Svec, J. Vacek, J. V. Chocholousová, A. JancarK, J. RybCek, K. Kosmider, I. G. Stará, P. Jelínek, I. Starý, *Nat. Chem.* **2017**, *9*, 213; d) T. G. Lohr, J. I. Urgel, K. Eimre, J. Liu, M. Di Giovannantonio, S. Mishra, R. Berger, P. Ruffieux, C. A. Pignedoli, R. Fasel, X. Feng, *J.*

Am. Chem. Soc. **2020**, *142*, 13565; e) X. Xu, K. Sun, A. Ishikawa, A. Narita, S. Kawai, *Angew. Chem., Int. Ed.* **2023**, *62*, e202302534.

[13] a) B. Schuler, S. Fatayer, F. Mohn, N. Moll, N. Pavlicek, G. Meyer, D. Peña, L. Gross, *Nat. Chem.* **2016**, *8*, 220; b) A. Shiotari, T. Nakae, K. Iwata, S. Mori, T. Okujima, H. Uno, H. Sakaguchi, Y. Sugimoto, *Nat. Commun.* **2017**, *8*, 16089; c) B. Mallada, B. De La Torre, J. I. Mendieta-Moreno, D. Nachtigallová, A. Matej, M. Matousek, P. Mutombo, J. Brabec, L. Veis, T. Cadart, M. Kotora, P. Jelínek, *J. Am. Chem. Soc.* **2021**, *143*, 14694; d) J. I. Mendieta-Moreno, B. Mallada, B. De La Torre, T. Cadart, M. Kotora, P. Jelínek, *Angew. Chem., Int. Ed.* **2022**, *61*, e202208010; e) F. Albrecht, S. Fatayer, I. Pozo, I. Tavernelli, J. Repp, D. Peña, L. Gross, *Science* **2022**, *377*, 298; f) E. Pérez-Elvira, A. Barragán, Q. Chen, D. Soler-Polo, A. Sánchez-Grande, D. J. Vicent, K. Lauwaet, J. Santos, P. Mutombo, J. I. Mendieta-Moreno, B. De La Torre, J. M. Gallego, R. Miranda, N. Martín, P. Jelínek, J. I. Urgel, D. Écija, *Nat. Synth.* **2023**, https://doi.org/10.1038/s44160-023-00390-8.

[14] a) M. Di Giovannantonio, R. Fasel, *J. Polym. Sci.* **2022**, *60*, 1814; b) M. Di Giovannantonio, J. I. Urgel, U. Beser, A. V. Yakutovich, J. Wilhelm, C. A. Pignedoli, P. Ruffieux, A. Narita, K. Müllen, R. Fasel, *J. Am. Chem. Soc.* **2018**, *140*, 3532; c) M. Di Giovannantonio, Q. Chen, J. I. Urgel, P. Ruffieux, C. A. Pignedoli, K. Müllen, A. Narita, R. Fasel, *J. Am. Chem. Soc.* **2020**, *142*, 12925; d) Z. Sun, Q. Ye, C. Chi, J. Wu, *Chem. Soc. Rev.* **2012**, *41*, 7857; e) A. Shimizu, S. Nobusue, H. Miyoshi, Y. Tobe, *Pure Appl. Chem.* **2014**, *86*, 517; f) Y. Tobe, *Chem. Rec.* **2015**, *15*, 86; g) T. Kubo, *Chem. Lett.* **2015**, *44*, 111; h) D. T. Chase, B. D. Rose, S. P. Mcclintock, L. N. Zakharov, M. M. Haley, *Angew. Chem., Int. Ed.* **2011**, *50*, 1127.

[15] a) L. Bartels, G. Meyer, K.-H. Rieder, D. Velic, E. Knoesel, A. Hotzel, M. Wolf, G. Ertl, *Phys. Rev. Lett.* **1998**, *80*, 2004. b) L. Gross, F. Mohn, N. Moll, P. Liljeroth, G. Meyer, *Science* **2009**, *325*, 1110.

[16] a) J. I. Urgel, H. Hayashi, M. Di Giovannantonio, C. A. Pignedoli, S. Mishra, O. Deniz, M. Yamashita, T. Dienel, P. Ruffieux, H. Yamada, R. Fasel, *J. Am. Chem. Soc.* **2017**, *139*, 11658; b) R. Zuzak, P. Brandimarte, P. Olszowski, I. Izydorczyk, M. Markoulides, B. Such, M. Kolmer, M. Szymonski, A. Garcia-Lekue, D. Sánchez-Portal, A. Gourdon, S. Godlewski, *J. Phys. Chem. Lett.* **2020**, *11*, 10290.

[17] Q. Zhong, K. Niu, L. Chen, H. Zhang, D. Ebeling, J. Björk, K. Müllen, A. Schirmeisen, L. Chi, *J. Am. Chem. Soc.* **2022**, *144*, 8214.

[18] a) S. Braverman, Y. Duar, *J. Am. Chem. Soc.* **2002**, *112*, 5830; b) P. Bhattacharya, M. Singha, E. Das, A. Mandal, M. Maji, A. Basak, *Tetrahedron Lett.* **2018**, *59*, 3033.

[19] K. Fukuda, T. Nagami, J.-Y. Fujiyoshi, M. Nakano, *J. Phys. Chem. A* **2015**, *119*, 10620.

[20] F. J. Giessibl, *Appl. Phys. Lett.* **2000**, *76*, 1470.

[21] A. V. Yakutovich, K. Eimre, O. Schütt, L. Talirz, C. S. Adorf, C. W. Andersen, E. Ditler, D. Du, D. Passerone, B. Smit, N. Marzari, G. Pizzi, C. A. Pignedoli, *Comput. Mater. Sci.* **2021**, *188*, 110165.

[22] S. P. Huber, S. Zoupanos, M. Uhrin, L. Talirz, L. Kahle, R. Häuselmann, D. Gresch, T. Müller, A. V. Yakutovich, C. W. Andersen, F. F. Ramirez, C. S. Adorf, F. Gargiulo, S. Kumbhar, E. Passaro, C. Johnston, A. Merkys, A. Cepellotti, N. Mounet, N. Marzari, B. Kozinsky, G. Pizzi, *Sci. Data* **2020**, *7*, 300.

[23] T. D. Kühne, M. Iannuzzi, M. Del Ben, V. V. Rybkin, P. Seewald, F. Stein, T. Laino, R. Z. Khaliullin, O. Schütt, F. Schiffmann, D. Golze, J. Wilhelm, S. Chulkov, M. H. Bani-Hashemian, V. Weber, U. Borstnik, M. Taillefumier, A. S. Jakobovits, A. Lazzaro, H. Pabst, T. Müller, R. Schade, M. Guidon, S. Andermatt, N. Holmberg, G. K. Schenter, A. Hehn, A. Bussy, F. Belleflamme, G. Tabacchi, et al., *J. Chem. Phys.* **2020**, *152*, 194103.

[24] J. Vandevondele, J. Hutter, *J. Chem. Phys.* **2007**, *127*, 114105.

[25] S. Goedecker, M. Teter, J. Hutter, *Phys. Rev. B* **1996**, *54*, 1703.

[26] J. P. Perdew, K. Burke, M. Ernzerhof, *Phys. Rev. Lett.* **1996**, *77*, 3865.

[27] S. Grimme, J. Antony, S. Ehrlich, H. Krieg, *J. Chem. Phys.* **2010**, *132*, 154102.

[28] F. Hanke, J. Björk, *Phys. Rev. B* **2013**, *87*, 235422.